

Stability Constrained Optimization in High IBR-Penetrated Power Systems—Part I: Constraint Development and Unification

Zhongda Chu, *Member, IEEE*, and Fei Teng, *Senior Member, IEEE*

Abstract—Maintaining power system stability is becoming more and more challenging due to the ever-increasing inverter-interfaced renewable penetration in power systems. To ensure system stability during system operation and to provide appropriate incentives in the future market-based stability maintenance framework, it is essential to develop a comprehensive set of power system stability constraints which can be incorporated into system operation, market design and planning problems. In this paper, different system stability issues, including synchronization, voltage and frequency stability, are investigated and the corresponding stability conditions are analytically formulated as system operation constraints. A unified framework is further proposed to represent the stability constraints in a general form and enables effective reformulation of the impedance-based stability metrics. All the constraints are converted into linear or Second-Order-Cone (SOC) form, which can be readily implemented in any optimisation-based applications, such as system scheduling, planning and market design, thus providing significant value for multiple system stability enhancement and studies.

Index Terms—Power system optimization, stability constraints, inverter-based resources

I. INTRODUCTION

Renewable Energy Sources (RES) have been massively integrated into the modern electric power system in the past few decades due to the concerns on environment and sustainability throughout the world. Being the key element for the interface between RES and the grid, the power electronic converters are anticipated to acquire a steadily increasing role along the trend of decarbonization. However, owing to the intermittent nature of the renewable energy and the distinguished features of the Inverter-Based Resources (IBR), which stem from their control interactions, zero inertia provision, limited Short Circuit Current (SCC) and reactive power supports, power systems are facing new challenges in system operation, security and stability [1]–[4].

Among all these challenges, the frequency and inertia issues were first reported and have drawn significant attention of the researchers [1], [5]. Unlike the conventional SGs, which store remarkable amount of kinetic energy in the rotating mass and provide large amount of rotational inertia to power systems through their synchronous nature, the RES are connected to the grid through power electronics inverters and either have no rotational inertia (PV) or the inertia is decoupled from the grid by the converters (wind generation) thus providing zero inertia to the system if no additional control algorithm is implemented. As a result, replacing the conventional SGs with IBR would gradually lead to low-inertia power systems, whose frequency stability may be jeopardized.

Another issue due to the high IBR penetration is the voltage stability and reactive power (current) supply in both transient and static stages. During fault conditions, large amount of reactive current is required by the system to maintain the voltages across the system and generate sufficient fault current within a short period such that the fault could be detected and isolated by the protection system. In the UK, it is predicted by National Grid that with the increasing penetration of IBR, the Short Circuit Current (SCC) in most of the areas declines to different extents depending on regional conditions in the next few years [6], which may lead to transient voltage instability. This is because of the limited SCC contribution from IBR, around 1-2 p.u. [7] compared with conventional SGs (5-10 p.u. [8]).

On the other hand, during normal operation and small disturbances, enough reactive power should also be injected to the grid to maintain system voltages and ensure static voltage stability. Conventionally, static voltage stability analysis is typically carried out at load buses while assuming that the voltages at SG buses can be well regulated [9]. Hence, the voltage stability is mainly influenced by the loading conditions in the system. However, with the increasing integration of Grid-FoLLowing (GFL) IBRs, the voltage stability at IBR buses needs to be reassessed. Different from the conventional SGs, the GFL IBRs operate as current sources, which can not control their terminal voltage directly and do not provide reactive power support inherently. As a result, the voltage stability at the IBR buses can not be maintained under improper operating conditions [10].

Challenges in the synchronization stability of IBR have also been identified in high IBR-penetrated systems where the system strength at IBR buses is low [11]. Unlike SGs whose synchronization dynamics is dominated by the swing equation, the IBR's synchronization behavior is determined by their control strategies. Although both GFL and Grid-ForMing (GFM) control mode may suffer from synchronization stability issues, the main research focus lies on that of GFL units when connected to weak or faulty grid, due to the existence of the Phase-Locked Loop (PLL) [12]. In weak grid condition, the bus voltage at the Point of Common Coupling (PCC) of IBR is heavily influenced by the current injection from the IBR to the grid, forming a positive feedback loop, which may destabilize the PLL stability [13]. Under severe grid fault, the loss of synchronization of the PLL-based GFL IBR is also a large threat to power system stability. This is because a stable operating point may not exist due to the severe voltage drop and even though the stable equilibrium point exists, the damping that attracts the system dynamics to this point may

be insufficient [14].

Measures in different respects have been taken to address the issues associated with the reduced system inertia and frequency stability. For frequency stability, the concept of virtual synchronous machine is introduced in [15] to provide primary reserve supporting the grid frequency dynamics. Approaches based on gain-scheduling are proposed for frequency regulation in [16], [17], where the signal of the product of frequency deviation and RoCoF is used to determine the virtual inertia and/or damping heuristically. Furthermore, [18] suggests an LQR-based adaptive VSM to choose the optimal inertia and damping according to the system disturbance. Recently, machine learning-based approaches, e.g., reinforcement learning, have also been proposed to design the frequency support controllers in a non-parametric manner [19], [20].

Regarding voltage stability, an optimal active and reactive power control strategy is proposed in [21] in order to improve the static voltage stability using the battery energy storage system at the selected critical buses. [22] proposes an optimal Static Voltage Stability Margin (SVSM) control model considering the uncertain wind generation where the complex nonlinear chance and variance constraints are dealt with by the sensitivity method. In [23], the impact of Doubly Fed Induction Generators (DFIG) on long-term voltage stability is analyzed and improved through the grid-side converter control, while considering the capability curve and the control limits. The authors in [10] introduce a grid-feeding converter voltage stability assessment method where the maximum power injection from the IBR to the grid is found to ensure the voltage stability.

To avoid loss of synchronism of wind turbine generation, the instability of grid side converters of wind turbines during very deep voltage sags is explored in [24], where a novel stability solution based on PLL frequency is proposed. In [25], an adaptive PLL that switches between first-order and second-order during the fault-occurring/-clearing transient, is proposed to preserve the transient stability of PLL. The dynamic synchronization mechanism is investigated in [26] where an active power balancing control scheme for wind generation system is proposed for the synchronization stability during grid fault. The authors in [27] identifies the necessary stability conditions of a GFL converter during asymmetrical fault and proposes a reduced-order model for analyzing its synchronizing interaction with the external network. [28], [29] study the impact of PLL dynamics and grid impedance on the stability of three-phase grid-connected inverters and utilize feedforward control and symmetrical control methods to improve the PLL stability under weak grid conditions respectively.

Most of the existing research tends to resolve those issues from the perspective of device-level control design, where the processes of parameter tuning and the assessment of the stability of the entire system can be difficult. Moreover, solely depending on device-level control may fail to maintain system stability, especially during the transient processes where the IBR currents reach their limits, and the global optimality may not be achieved without system-level regulations. For example, to ensure frequency security in a most cost-effective manner, different frequency services need to be coordinated and co-

optimized during the system scheduling process, while considering the device-level control strategies. Therefore, optimal solutions need system level coordination of different resources to ensure various stability and maximize economic profit.

To achieve this purpose, it is necessary to develop system stability constraints, which can be further incorporated into system level optimizations. Although some work has been done on the system level to address stability issues such as [30]–[32] on frequency and [33]–[35] on voltage stability, only a specific stability issue is studied and the interactions among different stability are not investigated due to the complicated dynamics of different stability phenomena. There still lacks a unified stability constrained optimization framework in power system which can simultaneously incorporate various stability constraints in high IBR-penetrated system.

Another challenge preventing stability constraints from being embedded into power system optimization models is the reformulation of complex stability criteria. Typically, the criteria for different stability are highly nonlinear or even derived without explicit expressions, and hence cannot be directly incorporated as constraints into system optimization models. To solve this problem, analytical approaches such as piecewise linearization have been applied to transform the nonlinear stability criteria into linear form [32], [36]. However, due to the intricate system dynamics, these methods may lead to overconservative results, compromising the economic benefit of the system. To achieve more accurate representation of the stability constraints, data-driven techniques such as decision trees and neural networks have been applied to formulate system stability constraints into optimization model [37]. However, drawbacks of the data-driven approaches involve lack of guarantees (conservativeness), and interpretability, which is critical for power system applications.

In this context, this paper focuses on power system stability issues due to high IBR-penetration, including frequency stability, synchronization stability and voltage stability. System-level stability constraints are developed and a unified framework is proposed to reformulate the highly nonlinear constraints into linear or SOC form by combining analytical and data-driven approaches. Note that the newly extended converter-driven and resonance stabilities [38] is not covered in this work, as on one hand, with limited research in this area, the system level indicators of these two types of stability are not clear and on the other hand they are more relevant to converter control design and less to the system level conditions. The main contributions of this paper include the following:

- a) Stability criteria in high IBR-penetrated power systems are analytically formulated as operational constraints. Depending on system impedance, power injections, generator status, these constraints cover frequency stability, synchronization stability and voltage stability and can be applied for any power system optimization model.
 - Synchronization stability of PLL-interfaced GFL IBRs is formulated as operational constraints and incorporated into the proposed framework, to ensure both the existence of equilibrium point and the small-signal synchronization stability.
 - Transient voltage stability constraints are developed based on short circuit currents and post fault voltages.

An SCC quantification method is proposed where the IBRs during grid fault are modeled as voltage-dependent current sources to account for the actual voltage drop at IBR terminals.

- b) A novel unified reformulation framework is proposed, which transforms the derived power system stability constraints into SOC form. It combines analytical derivation and data-driven approach to achieve both conservativeness and accuracy.

The rest of the paper is organized as follows. In Section II, different system stability constraints are developed, including synchronization and voltage stability of GFL IBRs, and system frequency stability. The resulting stability constraints are further converted to SOC or linear forms in Section III which can be directly included into power system optimization model. Section IV concludes the paper.

II. POWER SYSTEM STABILITY CONSTRAINT DEVELOPMENT

In this section, different stability constraints are derived analytically. Specifically, we focus on the synchronization and voltage stability of GFL IBRs, and system frequency stability. For the synchronization stability, the existence of equilibrium point, small-signal and transient stability are discussed, whereas for the voltage stability, both small-signal and transient stability are investigated. The system level frequency stability is assessed based on the security constraints specified by system operators, such as that of maximum RoCoF, frequency nadir and steady-state frequency.

Consider a power system having $n \in \mathcal{N}$ buses with $g \in \mathcal{G}$, $c_l \in \mathcal{C}_l$ and $c_m \in \mathcal{C}_m$ being the set of conventional Synchronous Generators (SGs), GFL and GFM inverter-based generators. $\Psi(g)$ and $\Phi(c)$ map the units in $g \in \mathcal{G}$ and $c \in \mathcal{C} = \mathcal{C}_l \cup \mathcal{C}_m$ to the corresponding bus indices respectively.

A. Synchronization Stability of IBRs

The IBR units are generally synchronized with the grid through one of the two methods, namely voltage-based grid synchronization (GFL control) and power-based synchronization (GFM control) [11]. The former relies on the estimation or measurement of the frequency and phase of the voltage at the point of common coupling which is achieved through the implementation of PLL, whereas the latter directly controls the phase of PCC voltage by regulating the IBR active power, such as $P-f$ droop control. Different research suggests that the GFL IBRs may suffer from synchronization instability under weak connection with the grid, under both small and large disturbances. To ensure the synchronization stability of GFL IBRs, the constraints corresponding to the existence of equilibrium point, small-signal and transient stability are developed in this subsection.

1) *Existence of equilibrium point*: To ensure the synchronization stability of IBRs, there should always exist an equilibrium point for both GFL and GFM IBRs.

The dynamics of a typical PLL structure in GFL IBRs can be described as:

$$\frac{d(\theta_{\Phi(c_l)}^{\text{pll}} - \theta_{\Phi(c_l)}^G)}{dt} = K_p v_q + \int K_i v_q \quad (1a)$$

$$v_q = V_{\Phi(c_l)}^G \sin(\theta_{\Phi(c_l)}^{\text{pll}} - \theta_{\Phi(c_l)}^G) + I_{c_l} Z_{\Phi(c_l)\Phi(c_l)} \sin(\phi_{c_l} + \phi_Z^G), \quad (1b)$$

where $\theta_{\Phi(c_l)}^{\text{pll}}$ and $\theta_{\Phi(c_l)}^G$ are the phase angles of PLL and grid voltage $V_{\Phi(c_l)}^G$; v_q is the q-axis component of PCC voltage; K_p and K_i are the PI control gains; ϕ_{c_l} and ϕ_Z^G denote the angle of IBR output current I_{c_l} defined on the PLL frame, and the angle of grid impedance.

At the equilibrium point of (1), $f^{\text{pll}} = f^G$, i.e., the GFL IBR is synchronized with the grid. Therefore, for stable operation, the PLL must be able to regulate v_q to zero. From (1b), one necessary condition (the existence of equilibrium points) of IBR synchronization stability can be derived as:

$$I_{c_l} \leq \frac{V_{\Phi(c_l)}^G}{Z_{\Phi(c_l)\Phi(c_l)} \sin(\phi_{c_l} + \phi_Z^G)}. \quad (2)$$

After eliminating the angle ϕ_{c_l} with its active and reactive power injection P_{c_l} , Q_{c_l} , (2) can be converted to:

$$\frac{V_{\Phi(c_l)}^G V_{\Phi(c_l)}}{Z_{\Phi(c_l)\Phi(c_l)}} \geq \cos \phi_Z^G Q_{c_l} + \sin \phi_Z^G P_{c_l}, \quad (3)$$

where $V_{\Phi(c_l)}$ is the voltage of PCC. Note that the above constraint is a necessary condition for IBR synchronization stability and should apply during both normal operation and grid fault.

2) *Small signal synchronization stability*: In weak grids (large grid impedance), the IBR PCC voltage can be significantly affected by the current injection into the grid, forming a self-synchronization loop (positive feedback) and hence undermining the GFL IBR synchronization stability. The method proposed in [39], [40] is adapted here where the small signal stability of PLL-based GFL IBRs is assessed through the generalized short circuit ratio (gSCR). It is defined as the minimum eigenvalue of extended admittance matrix, Y_{eq} :

$$\text{gSCR} = \lambda_{\min}(Y_{eq}) \quad (4a)$$

$$Y_{eq} = \text{diag} \left(\frac{V_{\Phi(c_l)}^2}{P_{c_l}} \right) Y_{red}, \quad (4b)$$

where $\text{diag} \left(\frac{V_{\Phi(c_l)}^2}{P_{c_l}} \right)$ is the diagonal matrix related to the GFL IBR terminal voltage and output power and Y_{red} is the reduced node admittance matrix after eliminating passive buses and infinite buses. It has been revealed that the smallest eigenvalue of Y_{eq} represents the connectivity of the network, and thus the grid voltage strength. Therefore, the small signal synchronization stability constraint can be then formulated as:

$$\text{gSCR} \geq \text{gSCR}_{\text{lim}}, \quad (5)$$

where gSCR_{lim} is the critical (minimum) gSCR that needs to be maintained to ensure the small signal stability of the GFL units. Furthermore, based on the assumption that the system voltages stay close to 1 p.u. during normal operation and small disturbances, the critical gSCR is an operation-independent

value, which can be determined offline with or without the detailed control parameters of the grid-following IBRs [40].

Impact of GFM units: Being modeled and controlled as voltage sources, the GFM converters improves the system strength, thereby enhancing the small-signal stability of power systems with large scale PLL-based GFL converters. GFM converters can be modeled as a voltage source in series with an admittance with large magnitude, which can be treated similar to conventional SGs for small-signal analysis (without saturation). Hence, the small-signal stability constraints considering the impact of GFM converters can be represented by [41]:

$$\text{gSCR} = \lambda_{\min} [\mathcal{R}_{C_m}(Y_{eq})] \geq \text{gSCR}_{\text{lim}}, \quad (6)$$

where $\mathcal{R}_{C_m}(Y_{eq})$ is a function to delete the row and the column corresponding to all GFM units in C_m .

3) *Large signal synchronization stability:* In addition to the small signal instability caused by weak grid connection, the IBR synchronization stability during grid faults should also be maintained. Various control methods have been proposed to enhance the transient synchronization stability of GFL IBRs during grid faults. Generally, this can be achieved through either active power adjustment or PLL parameter modification. With proper selection of these control schemes, the transient synchronization stability can be maintained during grid faults. For instance, by aligning the output current vector with the negative grid impedance, the transient stability can be always guaranteed with mathematical proof [42]. Since the normal operating conditions have little impact on the stability performance based on these control methods, the transient stability constraints during system operation is not considered in this work.

B. Voltage Stability

With the decline of conventional SGs and the corresponding reactive power and current support, system strength at the PCC of GFL IBRs decreases, which may bring voltage stability issues if left unmanaged.

1) *Small signal (static) voltage stability:* The static voltage stability constraints previously derived in [35] are briefly presented here. Based on system power flow equation, the

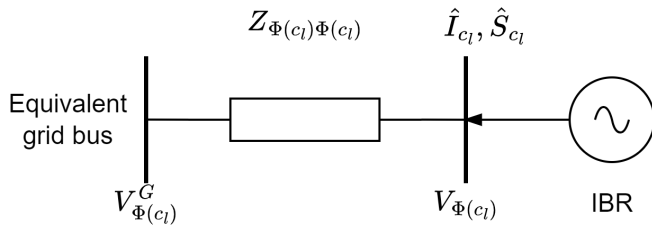


Fig. 1: Equivalent circuit of a general AC system seen from an IBR bus.

current injection at the PCC of GFL IBR is expressed as:

$$V_{\Phi(c_l)} = \underbrace{\sum_{g \in \mathcal{G} \cup C_m} Z_{\Phi(c_l)\Psi(g)} I_g}_{V_{\Phi(c_l)}^G} + Z_{\Phi(c_l)\Phi(c_l)} \underbrace{\left(I_{c_l} + \sum_{c'_l \in \mathcal{C}, c'_l \neq c_l} \frac{Z_{\Phi(c_l)\Phi(c'_l)}}{Z_{\Phi(c_l)\Phi(c_l)}} I_{c'_l} \right)}_{\hat{I}_{c_l}}. \quad (7)$$

The above relationship can be represented by an equivalent two-bus system with one bus being Bus $\Phi(c_l)$ and the other bus representing the rest of the system, i.e., the equivalent grid bus with its voltage $V_{\Phi(c_l)}^G$, formed by all the voltage sources in the system, as shown in Fig. 1. The IBR unit is connected to the grid bus through the impedance $Z_{\Phi(c_l)\Phi(c_l)}$ with an equivalent current injection, \hat{I}_{c_l} . This equivalent current includes the current from IBR c_l and the currents from other IBRs referred to Bus $\Phi(c_l)$ by the impedance ratio. The equivalent complex power injection from IBR c_l is then calculated by combining (7) and $\hat{S}_{c_l} = \hat{P}_{c_l} + j\hat{Q}_{c_l}$, which leads to:

$$\begin{bmatrix} \hat{P}_{c_l} \\ \hat{Q}_{c_l} \end{bmatrix} = \begin{bmatrix} \frac{|V_{\Phi(c_l)}| |V_{\Phi(c_l)}^G| \sin \theta_{c_l}}{|Z_{\Phi(c_l)\Phi(c_l)}|} \\ \frac{|V_{\Phi(c_l)}|^2 - |V_{\Phi(c_l)}| |V_{\Phi(c_l)}^G| \cos \theta_{c_l}}{|Z_{\Phi(c_l)\Phi(c_l)}|} \end{bmatrix}, \quad (8)$$

with $\theta_{c_l} = \angle V_{\Phi(c_l)} - \angle V_{\Phi(c_l)}^G$ being the angle difference between the PCC voltage and the equivalent grid voltage. Eliminating the angle θ_{c_l} gives the closed form solution of $V_{\Phi(c_l)}$:

$$|V_{\Phi(c_l)}|^2 = \frac{|V_{\Phi(c_l)}^G|^2}{2} + \hat{Q}_{c_l} |Z_{\Phi(c_l)\Phi(c_l)}| \pm \sqrt{\Delta}, \quad (9)$$

where

$$\Delta = \frac{|V_{\Phi(c_l)}^G|^4}{4} - \hat{P}_{c_l}^2 |Z_{\Phi(c_l)\Phi(c_l)}|^2 + \hat{Q}_{c_l} |Z_{\Phi(c_l)\Phi(c_l)}| |V_{\Phi(c_l)}^G|^2. \quad (10)$$

In order to ensure the voltage stability of the GFL IBR c_l , real roots of $|V_{\Phi(c_l)}|$ should exist, i.e., $\sqrt{\Delta} \geq 0$, thus yielding the following voltage stability constraints in terms of the IBR maximum power transfer capability

$$\hat{P}_{c_l}^2 + \hat{Q}_{c_l}^2 \leq \left(\hat{Q}_{c_l} + \underbrace{\frac{|V_{\Phi(c_l)}^G|^2}{2|Z_{\Phi(c_l)\Phi(c_l)}|}}_{\Gamma_{c_l}} \right)^2, \quad (11)$$

where \hat{P}_{c_l} and \hat{Q}_{c_l} take the form:

$$\hat{P}_{c_l} = P_{c_l} + \sum_{c'_l \in \mathcal{C}, c'_l \neq c_l} \frac{|Z_{\Phi(c_l)\Phi(c'_l)}|}{|Z_{\Phi(c_l)\Phi(c_l)}|} P_{c'_l} \quad (12a)$$

$$\hat{Q}_{c_l} = Q_{c_l} + \sum_{c'_l \in \mathcal{C}, c'_l \neq c_l} \frac{|Z_{\Phi(c_l)\Phi(c'_l)}|}{|Z_{\Phi(c_l)\Phi(c_l)}|} Q_{c'_l}. \quad (12b)$$

This voltage stability condition illustrates that the equivalent active power injection of IBR c_l is limited by an upper bound depending on short circuit capacity $\left(|V_{\Phi(c_l)}^G|^2 / |Z_{\Phi(c_l)\Phi(c_l)}| \right)$ at Bus $\Phi(c_l)$ if no reactive power is provided by IBR. At weak points of the system where $|Z_{\Phi(c_l)\Phi(c_l)}|$ is large, the

active power injection from IBRs may have to be set smaller than the rated or even the available power to maintain voltage stability. Furthermore, it is also shown in (11) that properly setting IBR reactive power injection would allow more active power to be transferred.

Impact of reactive power droop control Implemented with Q-V droop control, IBRs are able to support the PCC voltage magnitude by providing dynamic voltage support to the grid during system disturbance. However, the Q-V droop control does not change the voltage stability condition defined in (11), since this relationship should be maintained during steady state to achieve the power delivery. Moreover, a voltage deadband, e.g., [0.95, 1.05] is typically implemented in the Q-V droop control and hence the impact of Q-V droop control on the static voltage stability is not significant. After the equilibrium has been established, the Q-V droop control helps to maintain the PCC voltage if disturbances occur in the system, which is analyzed in the next section.

2) *Large signal (transient) voltage stability*: Due to the complexity and nonlinearity during the transient responses, transient voltage stability is typically assessed through time-domain simulations. In general, it is difficult to mathematically analyze the transient voltage stability and there lacks a standard, reliable and quantitative criterion to determine the transient voltage stability of power systems with high penetration of IBR. Few indices have been proposed to illustrate the transient voltage stability based on post fault voltage deviation [43], [44]. Moreover, these indices cannot be calculated analytically and often require time-domain simulations, thus not being able to be directly incorporated into system optimization models.

Instead, this work focuses on ensuring enough generation capacity in the system, such that adequate short circuit currents and the post-fault voltages at critical buses after severe faults can be maintained [45], [46]. Enough SCC ensures that the fault could be cleared by the protection devices within desired time and proper post-fault voltages prevent further generation tripping, which may lead to other instability and cascade failures. However, it should be noted that enough SCC and adequate post-fault voltage are not a necessary and sufficient condition for transient voltage stability, which is still an open question and is out of the scope of this research.

Combining the classic SCC superposition approach with the proposed model of IBRs during fault (voltage-dependent current sources) enables the SCC calculation in a general power system with both SGs and IBRs. Based on the superposition principle, the post-fault system operation can be viewed as the superposition of the pre- and 'pure'-fault conditions [47]. The SCC at the fault bus F can be computed through KCL in the 'pure'-fault system where the only sources are the current at the VSC buses and the fault bus [48]: **Define**

$$-V_F(0) = \sum_{c \in \mathcal{C}} Z_{F\Phi(c)}(I_{fc} - I_{Lc}) + Z_{FF}I_F'' \quad (13)$$

where $\Phi(c)$ maps the IBR $c \in \mathcal{C}$ to the corresponding bus index. Rearranging (13) yields the expression of the SCC at bus F as follows:

$$I_F'' = \frac{-V_F(0) - \sum_{c \in \mathcal{C}} Z_{F\Phi(c)}(I_{fc} - I_{Lc})}{Z_{FF}}. \quad (14)$$

IBRs are required to provide SCC according to their terminal voltage drop, which can be modeled by voltage dependent current sources. According to the grid code of UK national grid ESO [46], reactive current of full capacity (1.0 - 1.5 p.u.) is required from the GFM IBRs when their terminal voltages drop to zero, to support the post fault voltages and the system protection. Therefore, the fault current from IBR $c \in \mathcal{C}$ can be expressed as follows:

$$I_{fc} = -d_c \underbrace{(V_{\Phi(c)} - V_{\Phi(c)}(0))}_{\Delta V_{\Phi(c)}}, \quad (15)$$

where d_c is the reactive current droop gain; $V_{\Phi(c)}$ and $V_{\Phi(c)}(0)$ are the post-fault and pre-fault voltage at bus $\Phi(c)$. Based on the superposition principle, the voltage drop at bus $\Phi(c)$, $\Delta V_{\Phi(c)}$ can be derived:

$$\Delta V_{\Phi(c)} = Z_{\Phi(c)\Phi(c)}(I_{fc} - I_{Lc}) + Z_{F\Phi(c)}I_F''. \quad (16)$$

Equation (16) is essentially an implicit function of $\Delta V_{\Phi(c)}$, due to the dependence of I_{fc} on $\Delta V_{\Phi(c)}$. By inserting (15) into (16) and neglecting the pre-fault load current, the following expression of $\Delta V_{\Phi(c)}$ is obtained:

$$\Delta V_{\Phi(c)} = \frac{Z_{F\Phi(c)}I_F''}{1 + d_c Z_{\Phi(c)\Phi(c)}}. \quad (17)$$

Combining (14), (15) and (17) gives the SCC at fault bus F :

$$I_F'' = \frac{-V_F(0) + \sum_{c \in \mathcal{C}} Z_{F\Phi(c)}I_{Lc}}{Z_{FF} - \sum_{c \in \mathcal{C}} \frac{Z_{F\Phi(c)}^2}{1/d_c + Z_{\Phi(c)\Phi(c)}}}. \quad (18)$$

As it is the reactive component of the SCC that matters, the active load current is neglected, leading to the following SCC constraint:

$$\left| I_F'' \right| = \frac{V_F(0)}{Z_{FF} - \sum_{c \in \mathcal{C}} \frac{Z_{F\Phi(c)}^2}{1/d_c + Z_{\Phi(c)\Phi(c)}}} \geq I_{F\text{lim}}''. \quad (19)$$

Note that the above SCC expression reduces to the conventional formula, $V_F(0)/Z_{FF}$, if the SCC from IBR units are neglected, i.e., $d_c = 0$.

Moreover, to prevent generation units from disconnecting, the post-fault voltage at their terminals should be maintained above a certain level according to fault ride through requirement of the grid code, for instance limits of 0.05 - 0.3 p.u. for synchronous units and 0.05 - 0.15 p.u. for IBRs are specified in [49]. Hence, substituting (19) into (17) gives the post-fault voltage constraint at IBR buses in close form:

$$\begin{aligned} |\Delta V_{\Phi(c)}| &= \frac{V_F(0)Z_{F\Phi(c)}}{Z_{FF}(1 + d_c Z_{\Phi(c)\Phi(c)}) - \sum_c d_c Z_{F\Phi(c)}^2} \\ &\leq \Delta V_{\text{lim}}. \end{aligned} \quad (20)$$

Remarkably, there are grid codes in other areas with different requirements regarding the fault current contribution from IBR units, such as full capacity reactive current at 0.5 p.u. and higher terminal voltage drop [50]. Therefore, the fault current from IBRs as previously defined in (15) should be modified as:

$$I_{fc} = \min \{ I_c^{\text{max}}, d_c |\Delta V_{\Phi(c)}| \}. \quad (21)$$

In this case, a simple explicit expression of the SCC as in (18) may not be available due to the interdependence between the IBR fault currents and post-fault voltages. However, I_F'' can still be calculated in an iterative manner, given the system operating conditions. As for how it can be reformulates as a constraint and incorporated into optimization model, they are discussed in Section III.

C. Frequency Stability

Although frequency stability constraints do not involve system impedance, it closely relates to the status of SGs through the inertia provision, thus influencing system impedance and interacting with other stability constraints. Hence, the frequency stability constraints are also introduced here. A novel wind turbine SI control scheme is proposed in [32], which eliminates the secondary frequency dip due to WT overproduction and allows the WT dynamics to be analytically integrated into the system frequency dynamics. The frequency nadir constraint is formulated as:

$$HR \geq \frac{\Delta P_L^2 T_d}{4\Delta f_{lim}} - \frac{\Delta P_L T_d}{4} \left(D - \sum_{j \in \mathcal{F}} \gamma_j H_{s_j}^2 \right), \quad (22)$$

where H is the sum of conventional inertia H_c and SI of all the wind farms $\sum_j H_{s_j}$ with $j \in \mathcal{F}$ being the set of wind farms and R , T_d represent the system Primary Frequency Response (PFR) and its delivery time; ΔP_L , Δf_{lim} and D denote system disturbance, limit of frequency deviation and system damping. The last term can be interpreted as: SI provision from each wind farm introduces a negative damping to the system proportional to H_{s_j} with the coefficient being γ_j .

III. UNIFIED SOC REPRESENTATION OF SYSTEM STABILITY CONSTRAINTS

The impedance-based stability constraints introduced in previous section are highly nonlinear, which involve either matrix inverse or eigenvalue operation. Therefore, in order to incorporate these stability criteria into system scheduling framework, a unified reformulation method of these constraints which can be directly solved within the optimization model is desired. Remarkably, the developed system level stability constraints may involve uncertainties related to system dynamics, stemmed from various aspects, such as SG and line impedance, IBR parameters, system inertia. These uncertainties can be dealt with in the optimization problem by formulating the (distributionally-) robust chance constraints, which is not discussed in this work and will be considered in the future study.

A. General Expression of System stability Constraints

Rewrite the system stability constraints, (3), (6), (11) - (12), (19)-(20) and (34) derived in Section II in the following form:

$$\mathbf{g}_1(V, Z) = \frac{V_{\Phi(c_l)}^G V_{\Phi(c_l)}}{Z_{\Phi(c_l)\Phi(c_l)}} \geq \cos \phi_Z^G Q_{c_l} + \sin \phi_Z^G P_{c_l} \quad (23a)$$

$$\mathbf{g}_2(V, Z, P_{c_l}) = \lambda_{\min} [\mathcal{R}_{c_m}(Y_{eq})] \geq \text{gSCR}_{lim} \quad (23b)$$

$$\mathbf{g}_3(V, Z) = \frac{V_F(0)}{Z_{FF} - \sum_{c \in \mathcal{C}} \frac{Z_{F\Phi(c)}^2}{1/d_c + Z_{\Phi(c)\Phi(c)}}} \geq I_{F_{lim}}'' \quad (23c)$$

$$\mathbf{g}_4(V, Z) = \frac{-V_F(0)Z_{F\Phi(c)}}{Z_{FF}(1 + d_c Z_{\Phi(c)\Phi(c)}) - \sum_c d_c Z_{F\Phi(c)}^2} \geq -\Delta V_{lim} \quad (23d)$$

$$\mathbf{g}_5(\hat{P}_{c_l}, \hat{Q}_{c_l}, \Gamma_{c_l}) = (\hat{Q}_{c_l} + \Gamma_{c_l})^2 - \hat{P}_{c_l}^2 - \hat{Q}_{c_l}^2 \geq 0 \quad (23e)$$

$$\mathbf{g}_6(H, R, H_s) = HR - \frac{\Delta P_L^2 T_d}{4\Delta f_{lim}} - \frac{\Delta P_L T_d}{4} \left(D - \sum_{j \in \mathcal{F}} \gamma_j H_{s_j}^2 \right) \geq 0 \quad (23f)$$

where \hat{P}_{c_l} , \hat{Q}_{c_l} and Γ_{c_l} in (23e) are expressed by the equality constraints as follows:

$$\mathbf{h}_1(\hat{P}_{c_l}, P_{c_l}, Z) = \hat{P}_{c_l} - P_{c_l} - \sum_{c'_l \in \mathcal{C}, c'_l \neq c_l} \frac{|Z_{\Phi(c_l)\Phi(c'_l)}|}{|Z_{\Phi(c_l)\Phi(c_l)}|} P_{c'_l} = 0 \quad (24a)$$

$$\mathbf{h}_2(\hat{Q}_{c_l}, Q_{c_l}, Z) = \hat{Q}_{c_l} - Q_{c_l} - \sum_{c'_l \in \mathcal{C}, c'_l \neq c_l} \frac{|Z_{\Phi(c_l)\Phi(c'_l)}|}{|Z_{\Phi(c_l)\Phi(c_l)}|} Q_{c'_l} = 0 \quad (24b)$$

$$\mathbf{h}_3(V, Z) = \Gamma_{c_l} - \frac{|V_{\Phi(c_l)}^G|^2}{2|Z_{\Phi(c_l)\Phi(c_l)}|} = 0. \quad (24c)$$

The inequality constraints defined in (23) and equality ones in (24) ensure the concerned stability of systems with high IBR-penetration. All of them, except the frequency nadir constraint (23f), are system strength (impedance)-related, which makes them highly-nonlinear and involves either matrix inverse or eigenvalue operation with decision-dependence. Hence, it is generally complicated to incorporate them into MILP- or MISOCP-based system scheduling models. In order to achieve this, constraints (23a) - (23f) are first expressed in a general form:

$$\mathbf{g}_i(X_i) \geq \mathbf{g}_{i_{lim}}, \quad i \in \{1, 2, 3, 4, 5, 6\}, \quad (25)$$

where X_i is the decision variable in system optimization model and $\mathbf{g}_{i_{lim}} \in \mathbb{R}$ can be expressed as:

$$\mathbf{g}_{1_{lim}} = \max\{\cos \phi_Z^G Q_c + \sin \phi_Z^G P_c\} \approx 1 \quad (26a)$$

$$\mathbf{g}_{2_{lim}} = \text{gSCR}_{lim} \quad (26b)$$

$$\mathbf{g}_{3_{lim}} = I_{F_{lim}}'' \quad (26c)$$

$$\mathbf{g}_{4_{lim}} = -\Delta V_{lim} \quad (26d)$$

$$\mathbf{g}_{5_{lim}} = 0 \quad (26e)$$

$$\mathbf{g}_{6_{lim}} = 0. \quad (26f)$$

The approximation in (26a) is conservative and it holds because the output of GFL devices during normal operation is dominated by active power and $\sin \phi_Z^G \gg \cos \phi_Z^G$ in transmission systems. As a result, $\mathbf{g}_{i_{lim}}$, $\forall i$ are constants regardless of the operating conditions.

B. Connecting Stability Constraints with Decision Variables

Since the elements in the system impedance matrix Z are typically not decision variables in most of power system optimization problems, it is necessary to express the impedance matrix with the decision variables in an explicit form, such that the stability constraints can be maintained in the optimization model.

Given the system operating condition, i.e., the status of SGs, x_g , and the online percentage of GFM α_{c_m} , the system impedance and admittance matrix in \mathbf{g}_1 and \mathbf{g}_2 can be calculated by:

$$Z = Y^{-1} \quad (27a)$$

$$Y = Y^0 + Y^g, \quad (27b)$$

where Y^0 is the admittance matrix of the transmission lines only; Y^g denotes the additional Y matrix increment due to reactance of SGs and GFM IBRs. The elements in Y^g can be further expressed as:

$$Y_{ij}^g = \begin{cases} \frac{1}{X_g} x_g & \text{if } i = j \wedge \exists g \in \mathcal{G}, \text{ s.t. } i = \Psi(g) \\ \frac{1}{X_{c_m}} \alpha_{c_m} & \text{if } i = j \wedge \exists c_m \in \mathcal{C}_m, \text{ s.t. } i = \Psi(c_m) \\ 0 & \text{otherwise.} \end{cases} \quad (28)$$

The above equation manifests the contribution of SGs and GFM units to system voltage strength, since they are modeled as voltage sources behind impedances under steady state and small signal disturbances [41]. It is further assumed that the voltage magnitudes during normal operation, $V_{\Phi(c)}^G$, $V_{\Phi(c)}$ in (23a), (23b) and $V_F(0)$ in (23c), (23d) equal to 1 p.u.. Hence, \mathbf{g}_1 becomes a function of x_g and α_{c_m} , i.e., $\mathbf{X}_1 = [x_1, \dots, x_g, \dots, x_{|\mathcal{G}|}, \alpha_{c_1}, \dots, \alpha_{c_m}, \dots, \alpha_{|\mathcal{C}_m|}]$. Additionally, \mathbf{g}_2 also depends on the output power of GFL IBRs as defined in (4b). As a result, \mathbf{X}_2 can be written as $[x_1, \dots, x_g, \dots, x_{|\mathcal{G}|}, \alpha_{c_1}, \dots, \alpha_{c_m}, \dots, \alpha_{|\mathcal{C}_m|}, P_{c_1}, \dots, P_{c_l}, \dots, P_{|\mathcal{C}_l|}]$.

On the other hand, during transient processes, both GFM and GFL IBRs are controlled to inject reactive current depending on their terminal voltages, which are modeled as voltage-dependent current sources (15). Therefore, the matrix Y^g used to calculate \mathbf{g}_3 and \mathbf{g}_4 only includes the impedances from SGs and the contribution on system SCC and post-fault voltage from IBRs is modeled through the droop control. To further account for the variation of IBR online capacity due to the renewable resource variation, the IBR droop control gain, d_c , is replaced by $\alpha_c d_c$ with the coefficient α_c , $c \in \mathcal{C}$ representing the online percentage of IBR unit c . Therefore, \mathbf{X}_3 and \mathbf{X}_4 can be expressed as, $\mathbf{X}_i = [x_1, \dots, x_g, \dots, x_{|\mathcal{G}|}, \alpha_1, \dots, \alpha_c, \dots, \alpha_{|\mathcal{C}|}]$, $i \in \{3, 4\}$. As for \mathbf{g}_5 and \mathbf{g}_6 , they are explicit functions of the decision variables, i.e., $\mathbf{X}_5 = [\hat{P}_{c_l}, \hat{Q}_{c_l}, \Gamma_{c_l}]$ and $\mathbf{X}_6 = [H, R, H_s]$.

It should be noted that $x_g, \forall g \in \mathcal{G}$ can be viewed as binary decision variables, whereas for the IBRs, their operating conditions are determined by the current available wind/solar resources rather than the system operator. Therefore, the scenario-dependent parameter $\alpha_c \in [0, 1], \forall c \in \mathcal{C}$ is introduced to represent the percentage of IBRs' online capacity. The approach proposed in [51] and [52] is used in this paper where the online IBR capacity is estimated given the current available power based on historical data. Although there are

also some direct approaches to monitor or estimate the online capacity of the IBRs and could potentially provide more accurate results, it is out of the scope of this paper and is not discussed in more detail.

C. SOC Representation of Stability Constraint Boundary

It is understandable that due to the complex expression of \mathbf{g}_i and especially their dependence on the discrete variables, x_g through the matrix inverse and eigenvalue operations, it is general difficult to deal with those constraints in an optimization problem. In the following, a unified framework that can effectively reformulate the stability constraints, in a general way, to fit any typical power system optimization model is presented.

The target of the stability constraint reformulation is to describe the boundary of the stability feasible region through an SOC relationship. Although the SOC form is chosen because it is the most general constraints whose mixed-integer programming can be efficiently solved by commercial solvers, the proposed method can also be applied to obtain constraints in linear or even semidefinite form.

The estimated expressions of the nonlinear functions \mathbf{g}_i can be defined as follows:

$$\tilde{\mathbf{g}}_i(\mathbf{X}_i) = \mathbf{c}_i \mathbf{X}_i + \mathbf{d}_i - \|\mathbf{A}_i \mathbf{X}_i + \mathbf{b}_i\|, \quad (29)$$

where $\tilde{\mathbf{g}}_i$ is the estimated function of \mathbf{g}_i in SOC form and the matrices $\mathbf{A}_i \in \mathbb{R}^{j \times \dim(\mathbf{X}_i)}$, $\mathbf{b}_i \in \mathbb{R}^j$, $\mathbf{c}_i \in \mathbb{R}^{1 \times \dim(\mathbf{X}_i)}$ and $\mathbf{d}_i \in \mathbb{R}$ are parameters to describe the shape and position of the SOC. The value of j is a degree of freedom that should be chosen for the best fit. A larger j may yield more accurate description of the original nonlinear relationship, but result in more parameters and computational burden. By substituting (29) into (25), the system stability constraints can also be converted to SOC form straightforwardly:

$$\|\mathbf{A}_i \mathbf{X}_i + \mathbf{b}_i\| \leq \mathbf{c}_i \mathbf{X}_i + (\mathbf{d}_i - \mathbf{g}_{i_{\text{lim}}}). \quad (30)$$

In order to find the SOC parameters $\mathcal{K} = \{\mathbf{A}_i, \mathbf{b}_i, \mathbf{c}_i, \mathbf{d}_i\}, \forall i$ that can best describe the boundary of the system stability feasible region, the following boundary-aware optimization is proposed:

$$\min_{\mathcal{K}} \sum_{\omega^i \in \Omega_2^i} \left(\mathbf{g}_i^{(\omega^i)} - \tilde{\mathbf{g}}_i^{(\omega^i)} \right)^2 \quad (31a)$$

$$\text{s.t. } \tilde{\mathbf{g}}_i^{(\omega^i)} < \mathbf{g}_{i_{\text{lim}}}, \forall \omega^i \in \Omega_1^i \quad (31b)$$

$$\tilde{\mathbf{g}}_i^{(\omega^i)} \geq \mathbf{g}_{i_{\text{lim}}}, \forall \omega^i \in \Omega_3^i, \quad (31c)$$

with $\omega^i = \{\mathbf{X}_i^{(\omega^i)}, \mathbf{g}_i^{(\omega^i)}\} \in \Omega^i$ denoting the entire data set corresponding to stability constraint i . It is generated by evaluating \mathbf{g}_i in representative system conditions. For the SGs, all the possible generator combinations are considered, whereas for the continuous parameters $\alpha_c \in [0, 1]$, there are infinite possible conditions in theory. To obtain the data set with a finite size, the interval is evenly divided into n_c regions, $\forall c \in \mathcal{C}$, each of which is represented by its mean value. Hence, the total size of Ω^i is $2^{|\mathcal{G}|} \cdot n_c^{|\mathcal{C}|}$. The sets Ω_1^i , Ω_2^i and Ω_3^i are the subsets of Ω^i , whose relationship is defined as below:

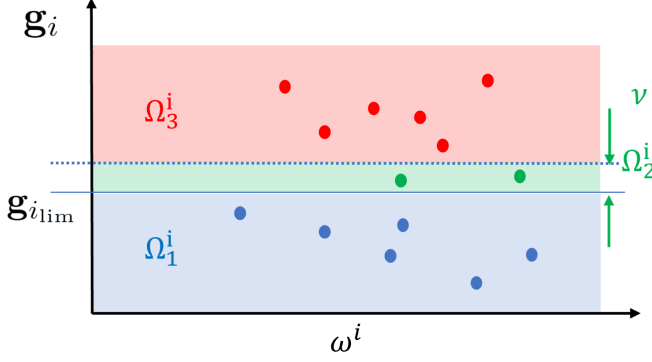


Fig. 2: Relationship of different data set.

$$\Omega^i = \Omega_1^i \cup \Omega_2^i \cup \Omega_3^i \quad (32a)$$

$$\Omega_1^i = \left\{ \omega^i \in \Omega^i \mid \mathbf{g}_i^{(\omega^i)} < \mathbf{g}_{i\text{lim}} \right\} \quad (32b)$$

$$\Omega_2^i = \left\{ \omega^i \in \Omega^i \mid \mathbf{g}_{i\text{lim}} \leq \mathbf{g}_i^{(\omega^i)} < \mathbf{g}_{i\text{lim}} + \nu \right\} \quad (32c)$$

$$\Omega_3^i = \left\{ \omega^i \in \Omega^i \mid \mathbf{g}_{i\text{lim}} + \nu \leq \mathbf{g}_i^{(\omega^i)} \right\}, \quad (32d)$$

with ν being a constant parameter. An example of the relationship in (32) is demonstrated in Fig. 2. Given (31b) and (32b), all the data points whose real stability indices, $\mathbf{g}_i^{(\omega^i)}$ are smaller than the limits, can be identified correctly by the estimated function, $\tilde{\mathbf{g}}_i^{(\omega^i)}$. Ideally, it is also desired to correctly identify all the above-limit data points, which would make the problem become a classification model. However, this may cause infeasibility due to the restricted SOC structure defined in (29). Therefore, a parameter $\nu \in \mathbb{R}^+$ is introduced to define Ω_2^i and Ω_3^i as in (32c) and (32d). In this way, all the data points in Ω_3^i (red area) will be classified correctly and misclassification can only occur in Ω_2^i (green area), thus being conservative.

Furthermore, ν should be chosen as small as possible while ensuring the feasibility of (31). Note that only the errors of data points in Ω_2^i are penalized in the objective function (31a), since for the data points in Ω_1^i and Ω_3^i , as long as they are classified on the correct side of the limits, the errors are of no concern. As a result, the proposed method ensures accurate approximation within a narrow region around the limits (Ω_2^i) whereas the regression errors of the data points in the other two regions are insignificant. Note that although (31c) is a constraint in SOC form, (31b) is nonconvex and needs to be linearized. This may increase the computational burden of solving (31), however, since it is an offline process, the computational time is not an issue.

As the original relationship in \mathbf{g}_5 and \mathbf{g}_6 resembles to that of an SOC, the parameters $\mathcal{K}_i = \{A_i, b_i, c_i, d_i\}$, $i \in \{5, 6\}$ can be directly identified by transforming $\mathbf{g}_i \geq \mathbf{g}_{i\text{lim}}$ into SOC form. For $\mathbf{g}_5 \geq \mathbf{g}_{5\text{lim}}$, it can be converted to standard SOC form as follows:

$$\left\| \begin{bmatrix} \hat{P}_c \\ \hat{Q}_c \end{bmatrix} \right\|_2 \leq \hat{Q}_c + \Gamma_c. \quad (33)$$

The parameters $\{A_5, b_5, c_5, d_5\}$ can therefore be determined accordingly. For $\mathbf{g}_6 \geq \mathbf{g}_{6\text{lim}}$, the method proposed in [53] is

used to convert the frequency nadir constraint \mathbf{g}_6 to SOC form. The original constraint $\mathbf{g}_6 \geq \mathbf{g}_{6\text{lim}}$ can be rewritten as follows:

$$HR \geq \underbrace{\frac{\Delta P_L^2 T_d}{4\Delta f_{\text{lim}}} - \frac{\Delta P_L T_d D}{4}}_{x_1^2} + \frac{\Delta P_L T_d \sum_{j \in \mathcal{F}} \gamma_j H_{s_j}^2}{4}. \quad (34)$$

Being a constant, the ancillary variable x_1 is defined for the sole purpose of SOC reformulation. Additionally, since in real power systems, the relationship $\Delta P_L / \Delta f_{\text{lim}} > D$ always holds, x_1 is real and (34) is well defined, which enables to express the nadir constraint in SOC form as below:

$$\left\| \begin{bmatrix} 2x_1 \\ \sqrt{\Delta P_L T_d} \mathbf{H}_s \\ H - R \end{bmatrix} \right\|_2 \leq H + R \quad (35)$$

where $\mathbf{H}_s = [\sqrt{\gamma_1} H_{s_1} \quad \sqrt{\gamma_2} H_{s_2} \quad \dots \quad \sqrt{\gamma_{|\mathcal{F}|}} H_{s_{|\mathcal{F}|}}]^T$. Based on (35), the SOC parameters $\{A_6, b_6, c_6, d_6\}$ can be identified.

D. Linear Reformulation of Equality Constraints

It can be observed that the only nonlinear terms in (24) are those related to the impedance matrix, $|Z_{\Phi(c)\Phi(c')}|/|Z_{\Phi(c)\Phi(c)}|$ and $1/|Z_{\Phi(c)\Phi(c)}|$. However, different from the inequality constraints (25), where accurate approximation is only required in the area around the boundaries, the linearization of the equality constraints (24) are desired to be accurate for all the operating conditions. Hence, for the equality constraints, the method proposed in Section III-C does not apply, since the boundary to be identified does not exist. Instead, a standard least square regression is utilized to find the best linear expression that describes the relationship between $|Z_{\Phi(c)\Phi(c')}|/|Z_{\Phi(c)\Phi(c)}|$, $1/|Z_{\Phi(c)\Phi(c)}|$ and the decision variables x_g, α_{c_m} [35].

Taking $\mathbf{h}_1 = 0$ for instance, define its linearized expression as follows:

$$\hat{P}_{c_l} - P_{c_l} - \sum_{c'_i \in \mathcal{C}, c'_i \neq c_l} \left(\sum_{g \in \mathcal{G}} k_g^{c'_i} x_g + \sum_{c_m \in \mathcal{C}_m} k_{c_m}^{c'_i} \alpha_{c_m} + \sum_{m \in \mathcal{M}} k_m^{c'_i} \eta_m \right) P_{c'_i} = 0, \quad (36)$$

where $\mathcal{K} = \{k_g^{c'_i}, k_{c_m}^{c'_i}, k_m^{c'_i}\}$, $\forall g, c_m, m$ are the sets of linear coefficients corresponding to $|Z_{\Phi(c)\Phi(c')}|/|Z_{\Phi(c)\Phi(c)}|$ determined by solving the least square regression within the entire data set. To further account for the nonlinearity in the original relationship, the term η_m is added to describe the interactions between every two units in SGs and GFM IBRs, i.e., $m \in \mathcal{M} = \{m_1, m_2 \mid m_1, m_2 \in \mathcal{G} \cup \mathcal{C}_m\}$, which is defined as follows:

$$\eta_m = \begin{cases} x_{m_1} x_{m_2}, & \text{if } m_1, m_2 \in \mathcal{G} \\ x_{m_1} \alpha_{m_2}, & \text{if } m_1 \in \mathcal{G}, m_2 \in \mathcal{C}_m \\ \alpha_{m_1} \alpha_{m_2}, & \text{if } m_1, m_2 \in \mathcal{C}_m \end{cases}, \quad \forall m \in \mathcal{M}. \quad (37)$$

Note that since the 2nd order terms lead to accurate enough results, the higher order terms are neglected in order to achieve a balance between the accuracy and computational effort.

IV. CONCLUSION

This paper proposes a stability-constrained optimization framework in high IBR-penetrated power systems to ensure system stability and security. System stability constraints covering from IBR synchronization and voltage stability to frequency stability are developed analytically. For the IBR synchronization stability, system operational constraints of both equilibrium point existence and small-signal stability are derived. Voltage stability involves small-signal and transient stability constraints, the latter of which is characterized by the sufficiency of generating capacity to provide fault current and maintain post-fault voltages.

Depending on system impedance, generator status and operating point, the highly nonlinear stability constraints are further reformulated into SOC form through a unified boundary-aware data-driven approach to achieve accuracy and conservativeness. The resulting constraints can be incorporated into any general power system optimization model. Part II of this paper validates the developed constraints and investigates their potential application in system scheduling and stability market design.

REFERENCES

- [1] F. Milano, F. Dörfler, G. Hug, D. J. Hill, and G. Verbič, "Foundations and challenges of low-inertia systems," in *PSCC*, 2018.
- [2] F. Blaabjerg, R. Teodorescu, M. Liserre, and A. V. Timbus, "Overview of control and grid synchronization for distributed power generation systems," *IEEE Transactions on Industrial Electronics*, vol. 53, no. 5, pp. 1398–1409, Oct 2006.
- [3] A. Ulbig, T. S. Borsche, and G. Andersson, "Impact of low rotational inertia on power system stability and operation," *IFAC Proceedings Volumes*, vol. 47, no. 3, pp. 7290–7297, 2014.
- [4] J. M. Carrasco *et al.*, "Power-electronic systems for the grid integration of renewable energy sources: A survey," *IEEE Transactions on Industrial Electronics*, vol. 53, no. 4, pp. 1002–1016, June 2006.
- [5] P. Tielens and D. Van Hertem, "The relevance of inertia in power systems," *Renewable and Sustainable Energy Reviews*, vol. 55, pp. 999–1009, 2016. [Online]. Available: <https://www.sciencedirect.com/science/article/pii/S136403211501268X>
- [6] nationalgridESO, "System operability framework: Impact of declining short circuit levels," Tech. Rep., December 2018.
- [7] J. Jia, G. Yang, and A. H. Nielsen, "A review on grid-connected converter control for short-circuit power provision under grid unbalanced faults," *IEEE Transactions on Power Delivery*, vol. 33, no. 2, pp. 649–661, 2018.
- [8] "7 - short-circuit analysis techniques in large-scale ac power systems," in *Power Systems Modelling and Fault Analysis (Second Edition)*, second edition ed., N. Tleis, Ed. Academic Press, 2019, pp. 597 – 664.
- [9] T. Cutsem and C. Vournas, *Voltage Stability of Electric Power Systems*. Boston: Springer, 1998.
- [10] J. Chen, F. Milano, and T. O'Donnell, "Assessment of grid-feeding converter voltage stability," *IEEE Transactions on Power Systems*, vol. 34, no. 5, pp. 3980–3982, 2019.
- [11] X. Wang, M. G. Taul, H. Wu, Y. Liao, F. Blaabjerg, and L. Harnfors, "Grid-synchronization stability of converter-based resources—an overview," *IEEE Open Journal of Industry Applications*, vol. 1, pp. 115–134, 2020.
- [12] nationalgrid, "Performance of phase-locked loop based converters," System Operability Framework, UK, Tech. Rep., December 2017.
- [13] D. Dong, B. Wen, D. Boroyevich, P. Mattavelli, and Y. Xue, "Analysis of phase-locked loop low-frequency stability in three-phase grid-connected power converters considering impedance interactions," *IEEE Transactions on Industrial Electronics*, vol. 62, no. 1, pp. 310–321, 2015.
- [14] Q. Hu, L. Fu, F. Ma, and F. Ji, "Large signal synchronizing instability of pll-based vsc connected to weak ac grid," *IEEE Transactions on Power Systems*, vol. 34, no. 4, pp. 3220–3229, 2019.
- [15] H.-P. Beck and R. Hesse, "Virtual synchronous machine," in *2007 9th International Conference on Electrical Power Quality and Utilisation*, 2007, pp. 1–6.
- [16] J. Alipoor, Y. Miura, and T. Ise, "Power system stabilization using virtual synchronous generator with alternating moment of inertia," *IEEE Journal of Emerging and Selected Topics in Power Electronics*, vol. 3, no. 2, pp. 451–458, June 2015.
- [17] D. Li, Q. Zhu, S. Lin, and X. Y. Bian, "A self-adaptive inertia and damping combination control of vsg to support frequency stability," *IEEE Transactions on Energy Conversion*, vol. 32, no. 1, pp. 397–398, March 2017.
- [18] U. Markovic, Z. Chu, P. Aristidou, and G. Hug, "Lqr-based adaptive virtual synchronous machine for power systems with high inverter penetration," *IEEE Transactions on Sustainable Energy*, vol. 10, no. 3, pp. 1501–1512, 2019.
- [19] C. Chen, M. Cui, F. Li, S. Yin, and X. Wang, "Model-free emergency frequency control based on reinforcement learning," *IEEE Transactions on Industrial Informatics*, vol. 17, no. 4, pp. 2336–2346, 2021.
- [20] O. Stanojev, O. Kundacina, U. Markovic, E. Vrettos, P. Aristidou, and G. Hug, "A reinforcement learning approach for fast frequency control in low-inertia power systems," in *2020 52nd North American Power Symposium (NAPS)*, 2021, pp. 1–6.
- [21] O. B. Adewuyi, R. Shigenobu, K. Ooya, T. Senjyu, and A. M. Howlader, "Static voltage stability improvement with battery energy storage considering optimal control of active and reactive power injection," *Electric Power Systems Research*, vol. 172, pp. 303–312, 2019.
- [22] Y. Yang, S. Lin, Q. Wang, Y. Xie, M. Liu, and Q. Li, "Optimization of static voltage stability margin considering uncertainties of wind power generation," *IEEE Transactions on Power Systems*, pp. 1–1, 2022.
- [23] R. R. Londero, C. de Mattos Affonso, and J. P. A. Vieira, "Long-term voltage stability analysis of variable speed wind generators," *IEEE Transactions on Power Systems*, vol. 30, no. 1, pp. 439–447, 2015.
- [24] O. Göksu, R. Teodorescu, C. L. Bak, F. Iov, and P. C. Kjaer, "Instability of wind turbine converters during current injection to low voltage grid faults and pll frequency based stability solution," *IEEE Transactions on Power Systems*, vol. 29, no. 4, pp. 1683–1691, 2014.
- [25] H. Wu and X. Wang, "Design-oriented transient stability analysis of pll-synchronized voltage-source converters," *IEEE Transactions on Power Electronics*, vol. 35, no. 4, pp. 3573–3589, 2020.
- [26] H. Geng, L. Liu, and R. Li, "Synchronization and reactive current support of pmsg-based wind farm during severe grid fault," *IEEE Transactions on Sustainable Energy*, vol. 9, no. 4, pp. 1596–1604, 2018.
- [27] M. G. Taul, S. Golestan, X. Wang, P. Davari, and F. Blaabjerg, "Modeling of converter synchronization stability under grid faults: The general case," *IEEE Journal of Emerging and Selected Topics in Power Electronics*, vol. 10, no. 3, pp. 2790–2804, 2022.
- [28] X. Zhang, D. Xia, Z. Fu, G. Wang, and D. Xu, "An improved feed-forward control method considering pll dynamics to improve weak grid stability of grid-connected inverters," *IEEE Transactions on Industry Applications*, vol. 54, no. 5, pp. 5143–5151, 2018.
- [29] X. Zhang, S. Fu, W. Chen, N. Zhao, G. Wang, and D. Xu, "A symmetrical control method for grid-connected converters to suppress the frequency coupling under weak grid conditions," *IEEE Transactions on Power Electronics*, vol. 35, no. 12, pp. 13 488–13 499, 2020.
- [30] M. Tuo and X. Li, "Security-constrained unit commitment considering locational frequency stability in low-inertia power grids," *IEEE Transactions on Power Systems*, pp. 1–13, 2022.
- [31] Y. Wen, W. Li, G. Huang, and X. Liu, "Frequency dynamics constrained unit commitment with battery energy storage," *IEEE Transactions on Power Systems*, vol. 31, no. 6, pp. 5115–5125, 2016.
- [32] Z. Chu, U. Markovic, G. Hug, and F. Teng, "Towards optimal system scheduling with synthetic inertia provision from wind turbines," *IEEE Trans. Power Syst.*, vol. 35, no. 5, pp. 4056–4066, 2020.
- [33] N. Zhang, S. Wu, H. An, and X. Zhu, "Security-Constrained Unit Commitment for AC/DC Transmission Systems with Voltage Stability Constraint," *Journal of Electrical Engineering & Technology*, vol. 15, no. 6, pp. 2459–2469, Sep. 2020.
- [34] N. Zhang, Q. Zhou, and H. Hu, "Minimum frequency and voltage stability constrained unit commitment for ac/dc transmission systems," *Applied Sciences*, vol. 9, no. 16, 2019.
- [35] Z. Chu and F. Teng, "Voltage stability constrained unit commitment in power systems with high inverter-based generator penetration," *IEEE Transactions on Power Systems*, pp. 1–1, 2022.
- [36] L. Badesa, F. Teng, and G. Strbac, "Simultaneous scheduling of multiple frequency services in stochastic unit commitment," *IEEE Transactions on Power Systems*, vol. 34, no. 5, pp. 3858–3868, 2019.
- [37] S. Zhang, Z. Zhu, and Y. Li, "A critical review of data-driven transient stability assessment of power systems: principles, prospects and challenges," *Energies*, vol. 14, no. 21, p. 7238, 2021.
- [38] N. Hatziaargyriou, J. Milanovic, C. Rahmann, V. Ajjarapu, C. Canizares, I. Erlich, D. Hill, I. Hiskens, I. Kamwa, B. Pal, P. Pourbeik, J. Sanchez-

- Gasca, A. Stankovic, T. Van Cutsem, V. Vittal, and C. Vournas, "Definition and classification of power system stability – revisited & extended," *IEEE Transactions on Power Systems*, vol. 36, no. 4, pp. 3271–3281, 2021.
- [39] W. Dong, H. Xin, D. Wu, and L. Huang, "Small signal stability analysis of multi-infeed power electronic systems based on grid strength assessment," *IEEE Transactions on Power Systems*, vol. 34, no. 2, pp. 1393–1403, 2019.
- [40] C. Liu, H. Xin, D. Wu, and Y. Zhou, "Generalized operational short-circuit ratio for grid strength assessment in renewable power systems under non-rated operating conditions," *TechRxiv*, 2022.
- [41] C. Yang, L. Huang, H. Xin, and P. Ju, "Placing grid-forming converters to enhance small signal stability of pll-integrated power systems," *IEEE Transactions on Power Systems*, vol. 36, no. 4, pp. 3563–3573, 2021.
- [42] S. Ma, H. Geng, L. Liu, G. Yang, and B. C. Pal, "Grid-synchronization stability improvement of large scale wind farm during severe grid fault," *IEEE Transactions on Power Systems*, vol. 33, no. 1, pp. 216–226, 2018.
- [43] A. Boričić, J. L. R. Torres, and M. Popov, "Comprehensive review of short-term voltage stability evaluation methods in modern power systems," *Energies*, vol. 14, no. 14, 2021.
- [44] X. Li, Z. Li, L. Guan, L. Zhu, and F. Liu, "Review on transient voltage stability of power system," in *2020 IEEE Sustainable Power and Energy Conference (iSPEC)*, 2020, pp. 940–947.
- [45] M. H. Bollen, *Understanding Power Quality Problems: Voltage Sags and Interruptions*. Wiley-IEEE Press, 2000.
- [46] nationalgrid, "The grid code," UK, Tech. Rep., October 2022.
- [47] J. J. Grainger and W. D. Stevenson, *Power system analysis*. McGraw-Hill, 1994.
- [48] Z. Chu and F. Teng, "Short circuit current constrained uc in high ibg-penetrated power systems," *IEEE Transactions on Power Systems*, vol. 36, no. 4, pp. 3776–3785, 2021.
- [49] ENTSO-E, "Commission regulation (eu) 2016/631 of 14 april 2016 establishing a network code on requirements for grid connection of generators," UK, Tech. Rep., April 2016.
- [50] A. Q. Al-Shetwi, M. Hannan, K. P. Jern, M. Mansur, and T. Mahlia, "Grid-connected renewable energy sources: Review of the recent integration requirements and control methods," *Journal of Cleaner Production*, vol. 253, p. 119831, 2020.
- [51] L. Ruttledge, J. O’Sullivan, N. Miller, and D. Flynn, "Frequency response of power systems with variable speed wind turbines," in *2013 IEEE Power Energy Society General Meeting*, 2013.
- [52] F. Teng and G. Strbac, "Assessment of the role and value of frequency response support from wind plants," *IEEE Transactions on Sustainable Energy*, vol. 7, no. 2, pp. 586–595, 2016.
- [53] Z. Chu, N. Zhang, and F. Teng, "Frequency-constrained resilient scheduling of microgrid: A distributionally robust approach," *IEEE Transactions on Smart Grid*, pp. 1–1, 2021.